






RESEARCH ARTICLE | OCTOBER 22 2025

Integrated saturable-absorber-enhanced power booster for feedback sensitive on-chip pulsed lasers

D. Plaza-Vas  ; A. Quirce  ; E. Bente  ; N. Vermeulen  



APL Photonics 10, 100805 (2025)
<https://doi.org/10.1063/5.0296267>



Articles You May Be Interested In

Random number generator based on an integrated laser with on-chip optical feedback

Chaos (October 2017)

Noise amplification by chaotic dynamics in a delayed feedback laser system and its application to nondeterministic random bit generation

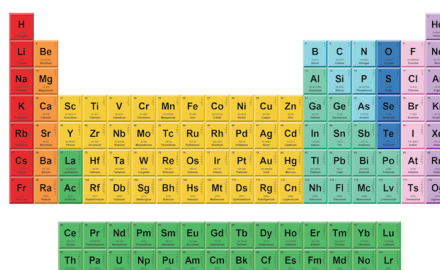
Chaos (December 2012)

Slope efficiency of integrated external cavity hybrid lasers: A general model and analysis

AIP Advances (March 2019)



Now Invent.™



*American Elements
 Opens a World of Possibilities*

...Now Invent!

www.americanelements.com

© 2021-2024 American Elements is a U.S. Registered Trademark

Integrated saturable-absorber-enhanced power booster for feedback sensitive on-chip pulsed lasers

Cite as: APL Photon. 10, 100805 (2025); doi: 10.1063/5.0296267

Submitted: 13 August 2025 • Accepted: 8 October 2025 •

Published Online: 22 October 2025



D. Plaza-Vas,^{1,2,3} A. Quirce,^{1,2} E. Bente,⁴ and N. Vermeulen^{1,a)}

AFFILIATIONS

¹Brussels Photonics (B-PHOT), Department of Applied Physics and Photonics, Vrije Universiteit Brussel (VUB), Pleinlaan 2, Brussels 1050, Belgium

²Instituto de Física de Cantabria (IFCA), Universidad de Cantabria (UC-CSIC), Avda. Los Castros s/n, Santander 39005, Spain

³Departamento de Física Moderna, Universidad de Cantabria (UC), Avda. Los Castros s/n, Santander 39005, Spain

⁴Technical University Eindhoven, Eindhoven 5612AZ, The Netherlands

^{a)}Author to whom correspondence should be addressed: Nathalie.Vermeulen@vub.be

ABSTRACT

The lack of optical isolators in photonic integrated circuits is a limiting factor for on-chip laser pulse amplification with a Semiconductor Optical Amplifier (SOA) power booster. Indeed, in the absence of optical isolation between an on-chip pulsed laser and the SOA power booster, amplified feedback signals can enter the laser cavity and destabilize the laser output. In this study, we propose an easy-to-implement and effective solution: a fully integrated Saturable Absorber (SA)-enhanced power booster that efficiently amplifies on-chip modelocked laser pulses while isolating the laser cavity from amplified feedback. Our booster design consists of an InP SOA preceded by a short (20–40 μm) InP SA. We demonstrate both experimentally and numerically that the presence of the short SA between the laser cavity and the SOA indeed prevents feedback-induced laser destabilization while still allowing efficient power amplification. The SA is found to induce a small power penalty of the order of 1 dB but, at the same time, allows using higher booster currents while maintaining stable laser operation. As such, our novel SA-enhanced booster design enables the on-chip generation of high-power stable laser pulses for a wide range of application domains.

© 2025 Author(s). All article content, except where otherwise noted, is licensed under a Creative Commons Attribution (CC BY) license (<https://creativecommons.org/licenses/by/4.0/>). <https://doi.org/10.1063/5.0296267>

INTRODUCTION

InP integrated photonics has emerged as a key technology for, among others, high-performance optical communication and signal processing, and allows integrating both active photonic devices, such as lasers and amplifiers, and passive components on a single chip.¹

Integrated InP Mode-Locked Lasers (MLLs) have garnered significant attention, as they enable on-chip generation of ultra-short pulses and Optical Frequency Combs (OFCs).^{2–5} Compared to traditional MLLs based on solid-state or fiber technologies, integrated MLLs, and particularly those based on passive modelocking by means of an intracavity Saturable Absorber (SA), offer a more compact and energy-efficient solution while maintaining high repetition rates and short pulses, as required for addressing the growing demands in optical communication and data processing.^{2,3,5}

Despite the advantages of integrated InP MLLs, a major challenge remains their limited pulse energy, typically on the order of 1 pJ.^{3,5} In InP Photonic Integrated Circuits (PICs), there is a trade-off between efficient light generation and inherently lossy waveguide transmission. Moreover, the high optical confinement in InP PICs, while beneficial for compactness and efficiency, also results in lower saturation power.⁵ The output pulses of an integrated InP MLL can be amplified by an on-chip InP Semiconductor Optical Amplifier (SOA). However, in the absence of optical isolation between the laser and the SOA, amplified feedback signals can enter the laser cavity and destabilize its output. Whether the feedback originates on-chip or off-chip, it will in either case be amplified by the SOA before entering the laser cavity. Controlled feedback can improve the lasing characteristics, e.g., by reducing phase noise and jitter.^{6,7} However, uncontrolled feedback can destabilize laser

sources, induce unwanted mode competition, and degrade overall system performance, leading to increased noise, linewidth broadening, and reduced efficiency.^{8–10} In the presence of an SOA amplifier, the feedback signal can become sufficiently strong to totally deteriorate the pulsed operation of integrated MLLs.

This stability problem could be solved by means of an optical isolator, but due to the lack of integrated optical isolators in PICs, alternative solutions have been explored. These include enhancing the intrinsic intracavity stability, implementing feedback suppression techniques, and leveraging non-reciprocal elements such as active modulators or nonlinear effects to avoid coupling of the back propagating signal into the laser cavity.^{10–14} Another interesting approach, proposed by Heck *et al.*,^{15,16} involves the use of a concatenated sequence of several SA and SOA sections integrated on a chip. They employed this concatenated structure in combination with a pulsed fiber laser and observed amplification and reshaping of the injected laser pulses.^{15,16} Although each of the solutions listed above shows promise, they often come with trade-offs in terms of complexity, power consumption, or effectiveness, and some were only tested with external lasers that were not integrated on chip. Hence, on-chip laser pulse amplification without destabilizing the laser itself remains a persistent challenge.

To tackle this challenge, we propose a custom, fully integrated power booster architecture for InP MLLs that enables efficient on-chip amplification of the laser pulses while suppressing detrimental feedback. The booster design is implemented using standard on-chip components available in commercial InP photonic foundries, ensuring compatibility with existing fabrication processes. Our booster design consists of a 500 μm -long InP SOA, preceded by a short (20–40 μm) InP SA. The presence of the short SA between the laser cavity and the SOA effectively prevents feedback-induced laser destabilization while still allowing efficient power amplification. Indeed, in view of the SA's nonlinear behavior, low-power feedback signals are absorbed in the SA, while the high-power pulses coming from the laser are almost fully transmitted by the SA. Our novel SA-enhanced booster architecture enables the generation of high-power on-chip pulses while maintaining stable laser operation, and as such, benefits several application domains, including optical communications, data processing, metrology, and light detection and ranging (LiDAR).

The structure of this paper is as follows: in the section Experimental Setup, we describe the InP PIC layout with MLLs combined with different booster configurations. In the section Experimental Results, we experimentally analyze the performance of our SA-enhanced custom booster architecture in comparison to conventional boosters. For this purpose, we study identical MLLs connected with either a “custom” booster or a conventional booster and investigate the output performance under diverse laser driving conditions. In addition, in the section Numerical Simulation Results, we present numerical simulation data for a conventional and a “custom” booster to confirm our experimental observations. Finally, we provide an overview of our findings and draw conclusions in the section Summary and Conclusions.

EXPERIMENTAL SETUP

To investigate the performance of the proposed SA-enhanced booster architecture, we prepared an InP PIC design with building

blocks as shown in Fig. 1(a) and submitted it to the Smart Photonics foundry for fabrication in a multi-project wafer run. The PIC contains several identical MLLs with a symmetrical racetrack resonator layout. The MLL cavity contains two 570 μm -long SOAs, with a 35 μm -long SA in between to establish modelocked operation, and also comprises a 50/50 multi-mode interference (MMI) coupler. The passive waveguide sections in the laser cavity have a nominal waveguide width of 2 μm . The cavity length equals 4700 μm , and the pulse repetition rate is ~ 17.2 GHz at 1550 nm. The identical MLLs are studied in three configurations: (a) *Reference*, i.e., the MLL is directly connected with an output waveguide toward the chip output facet; (b) *Conventional “Only SOA” Booster*, i.e., the MLL is followed by a 500 μm -long InP SOA booster and an output waveguide; and (c) *Custom Booster*, i.e., the MLL is followed by an SA-enhanced booster and an output waveguide, with the booster composed of a short InP SA (different lengths between 20 and 40 μm) and a 500 μm -long InP SOA next to it. The SA lengths are made as short as allowed by the foundry's fabrication rules to minimize the SA-induced power penalty (see further). The selected SOA length of 500 μm , which is of the same order of magnitude as the length of the intracavity SOAs, allows for significant gain while keeping the booster section compact. A picture of one of the fabricated PICs containing the structures mentioned earlier is presented in Fig. 1(b).

The output waveguides have an angled output facet with an anti-reflection (AR) coating to minimize reflections, and the emitted radiation is coupled to a lensed fiber (OZ Optics) that is AR-coated as well. The manufacturer of the lensed fiber specifies a residual reflection of around 0.25%. The fiber-coupled radiation is then directed via a fiber-based 50/50 power splitter to two different spectrum analyzers: we monitor the optical spectra and the output power with an Optical Spectrum Analyzer (OSA, APEX AP2083A) and its built-in power meter (PM), and we measure the radio frequency (RF) electrical spectra with a 35 GHz photodiode (PD, New Focus 1474-A) followed by a 26.5 GHz Electrical Spectrum Analyzer (ESA, Agilent E4407B). The driving currents for the SOAs and voltages for the SAs on the PIC are applied using electrical probes connected to a Thorlabs Pro8000 controller.

To compare the amplification and stability provided by the “only SOA” and “custom” boosters, we select the same driving conditions for all the MLLs and analyze the results obtained when sweeping the booster current from 0 to 90 mA. In the SA-enhanced “custom” boosters, the SA bias voltage is additionally varied from 0 to -4 V.

A representative optical spectrum of a reference MLL with SOAs 1 and 2 driven at 80 and 40 mA, respectively, and with the intracavity SA at -3 V bias, is shown in Fig. 1(c). As shown in Fig. 1(a), SOA1 is identified as the SOA that is closest to the MMI in the clockwise direction, i.e., the measurement direction and, therefore, the one that first encounters any feedback that propagates back into the laser cavity. Although the central emission wavelength of the laser SOAs is around 1550 nm, the MLL emission spectrum shows that the spectral absorption of the SA in the laser cavity causes a red-shift in the MLL emission toward 1575 nm. The spectral separation of the OFC comb lines in the emission spectrum is equal to the pulse repetition rate (17.2 GHz), which is determined by the MLL cavity length.

For completeness, we have measured the MLL pulse duration with a frequency resolved optical gating instrument (FROG,

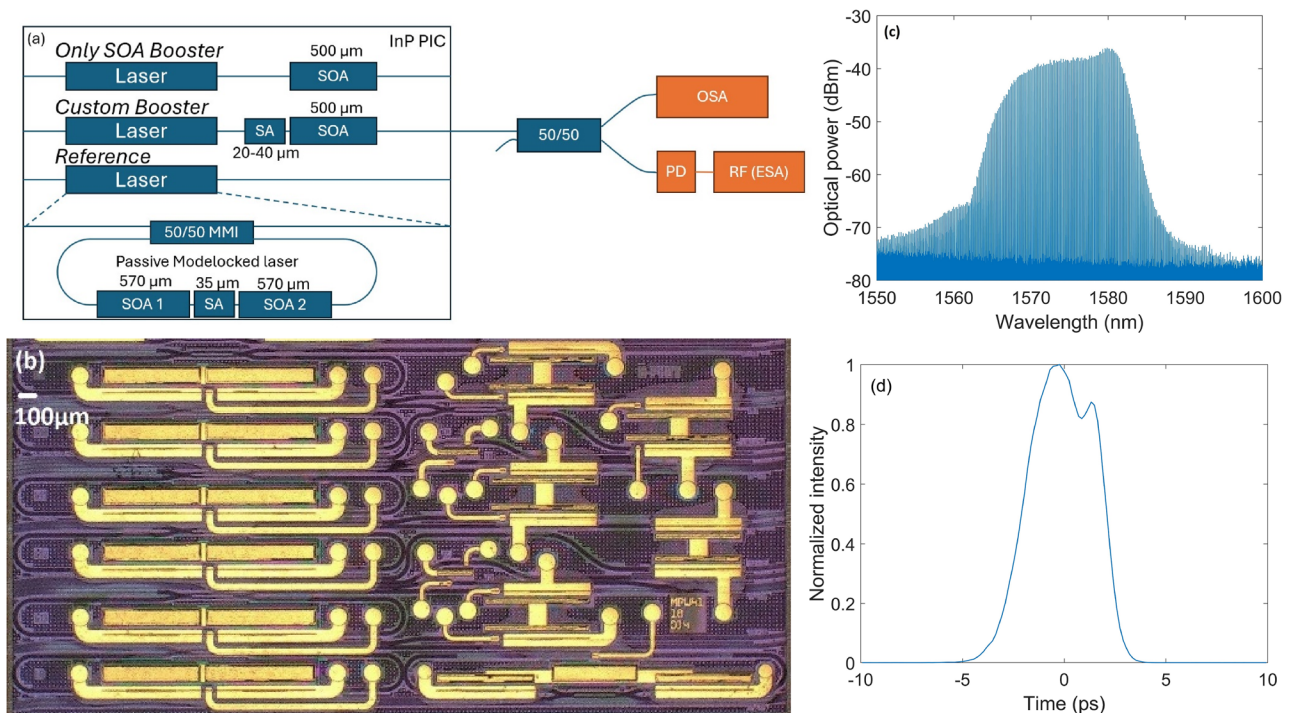


FIG. 1. (a) Schematic illustration of the PIC building blocks and the experimental setup. (b) Picture of a fabricated InP PIC containing MLLs and different booster structures. (c) Optical spectrum of a reference MLL driven at 80 mA (SOA1), 40 mA (SOA2), and -3 V (SA between SOA1 and SOA2). (d) Typical pulse shape showing a FWHM (full width at half maximum) pulse duration of 4.2 ps. The pulse shape has been measured with a FROG connected to the chip output with a 10 m fiber patch cord.

Coherent Solutions HR150). Figure 1(d) shows the pulse trace of one of the MLLs, exhibiting pulse durations of a few picoseconds. This measurement was achieved with an on-chip “custom” booster; no additional external amplification was needed to reach the minimally required power levels for the FROG (around 100 mW pulse peak power for this pulse repetition rate).

EXPERIMENTAL RESULTS

We start by studying the MLL followed by the conventional “Only SOA” booster and show that for such a configuration the laser can indeed become unstable due to feedback. The laser’s SOA1 and SOA2 are biased at 90 and 30 mA, respectively, and the intracavity SA is biased at -3 V in this and all the remaining cases presented in this section. Figure 2(a) shows the evolution of the RF peak output power with 5 MHz resolution around 17 GHz as the SOA booster current is increased from 0 to 90 mA. Our purpose is to evaluate relative changes in the modelocking stability. Here, we use the power of the highest RF peak measured with 5 MHz resolution as a relative measure for changes in modelocking stability and for changes in optical pulsing power. We note that an analogous approach for evaluating the modelocking stability was also used in Refs. 17 and 18. The resolution of 5 MHz was chosen so that we can simultaneously monitor the evolution of the modelocking stability and pulsing power.

The RF peak power curve in Fig. 2(a) is not monotonous, and starting from 60 mA booster current, the RF peak power suddenly

decreases. This strong drop in RF peak power is caused by the destabilization of the laser’s modelocked operation due to feedback, as explained further on. We investigate this further by studying the output at 40 and 80 mA booster currents, i.e., below and above the onset of destabilization, respectively. Figures 2(b) and 2(c) show the optical spectra at 40 and 80 mA booster currents, respectively, and Figs. 2(d) and 2(e) display the corresponding RF spectra.

At 40 mA current injection in the booster SOA, the optical spectrum in Fig. 2(b) shows an OFC envelope that, while not uniform, features a smooth, continuous shape. This is a sign of pulsing stability, as also demonstrated by the narrow RF peak in Fig. 2(d) with a 10 dB-bandwidth of 10 MHz. We note that Fig. 2(b) shows signs of having more than one OFC; this is a typical feature of ring MLLs operated at high currents.⁴

As the booster SOA current is further increased above 50 mA, the amplification becomes very strong, and this also implies that any feedback signal will gain strength before being coupled back into the laser cavity. This amplified feedback can disrupt the stable pulsing regime of the MLL. Indeed, Fig. 2(c) shows that the optical spectrum at 80 mA booster current is not as smooth as in Fig. 2(b), with multiple frequency lines emerging from the OFC envelope. The unstable laser operation at 80 mA booster current is further confirmed by the RF spectrum in Fig. 2(e), which shows a significantly broadened peak with a 10 dB-linewidth of ~ 380 MHz and a reduction in RF peak power by more than 14 dB. We note that the RF linewidths across the full range of booster currents are also displayed in Fig. 2(a), showing a sudden change around 50 mA booster

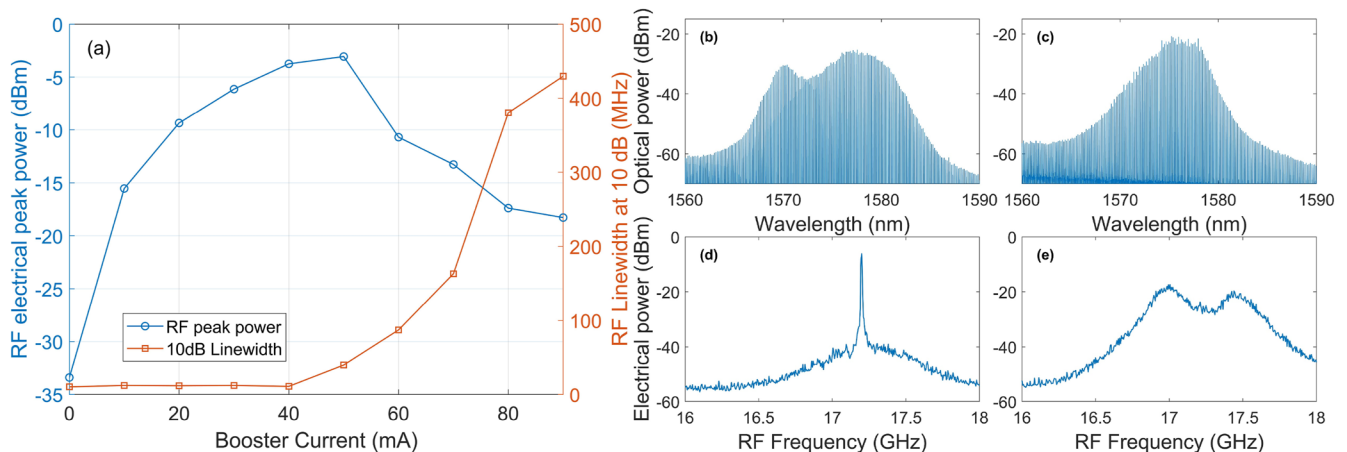


FIG. 2. RF peak power and RF linewidth around 17 GHz as a function of booster current for the MLL combined with the conventional “only SOA” booster (a). Output optical spectra at booster currents of 40 mA (b) and 80 mA (c). RF spectra with a resolution of 5 MHz at booster currents of 40 mA (d) and 80 mA (e).

current, as does the RF peak power. We also note that the 10 dB-linewidth of the individual comb lines broadens from 9 pm at 40 mA booster current to 12 pm at 80 mA.

The optical and RF spectra in Figs. 2(b)–2(e) validate that the evolution of the RF peak power in Fig. 2(a) provides an accurate and reliable representation of the evolution of the MLL’s stability and pulsing performance. To verify the origin of the feedback signal, we test the influence of the lensed fiber collecting the emitted radiation. When monitoring in real-time the RF and optical spectra while carefully misaligning the lensed fiber at the output facet, we observe that misaligning the position of the lensed fiber effectively suppresses the destabilizing feedback and restores stable pulsed operation. Hence, although we have only 0.25% residual reflection at the AR-coated lensed fiber, the resulting feedback signal can indeed destabilize the MLL, as it can get strongly amplified in the conventional “only SOA” booster before being coupled back into the laser cavity. Further analysis reveals no evidence that amplified spontaneous emission (ASE) from the booster SOA or on-chip back reflections would play a role in degrading the laser performance. In every tested unstable case, stability is recovered by deliberately misaligning the output lensed fiber such that the signal reflected back into the chip is strongly diminished.

Next, we compare the performances of the “only SOA” booster and “custom” booster configurations under the same laser driving conditions as used for Fig. 2, i.e., 90 and 30 mA for SOA1 and SOA2, respectively. Figure 3(a) presents the RF peak evolution as a function of booster SOA current for the “only SOA” booster (in dashed line) and for the “custom” booster with a 20 μm -long SA at different reverse bias voltages (in solid lines).

Figure 3(a) shows that for the SA-enhanced custom booster with 0 V bias voltage, lasing destabilization occurs at a similar booster current as for the conventional “only SOA” booster.

When progressively increasing the reverse bias voltage of the SA in the custom booster (and, therefore, also increasing its absorption), the custom booster configuration effectively suppresses feedback-induced instability and preserves stable pulsed lasing

operation across the entire current range of the booster SOA. This enhanced stability translates into improved RF peak power performance across the full booster SOA current range, with maximum RF peak powers reached at -2 and -3 V bias voltages (green and purple curves, respectively).

This trend is further supported by the optical spectra shown in Figs. 3(b)–3(e), representing the different cases in Fig. 3(a) at a fixed booster current of 90 mA. More specifically, we compare the output spectrum of the “only SOA” configuration [Fig. 3(b)] with the spectra of the “custom” booster with reverse bias voltages of 0 V [Fig. 3(c)], -1 V [Fig. 3(d)], and -3 V [Fig. 3(e)], measured at a booster current of 90 mA. A clear improvement in the smoothness of the spectral envelope is observed across the series from Figs. 3(b)–3(e). Indeed, the irregularities in the spectral envelope of Fig. 3(b) are progressively reduced from Figs. 3(c)–3(e), hence confirming MLL pulsing stability in the latter figure, in full agreement with the trend illustrated in Fig. 3(a). We note that the spectrum in Fig. 3(e) shows signs of having more than one OFC, similarly to the spectrum in Fig. 2(b). For completeness and in analogy with Fig. 2, we furthermore provide RF spectra in Figs. 3(f)–3(i) for the same configurations as in Figs. 3(b)–3(e). We observe narrowing of the RF spectra, starting from a linewidth of ~ 430 MHz in Fig. 3(f) down to a linewidth of 15 MHz in Fig. 3(i) for a reverse bias voltage of -3 V. A narrower RF linewidth accounts for stronger phase mode locking among the lasing modes, lower phase noise,¹⁹ and lower pulse-to-pulse timing jitter.²⁰

The results outlined above highlight both the effectiveness and tunability of the SA-enhanced custom booster configuration. By adjusting the SA bias voltage of the custom booster, it is possible to fine tune feedback isolation while significantly improving the MLL pulsing stability compared to the case where a conventional “only SOA” booster is employed. We point out that the SA-enhanced custom booster enables feedback isolation regardless of the origin of the feedback signal. A discussion on the output power of the different booster configurations will follow at the end of this section.

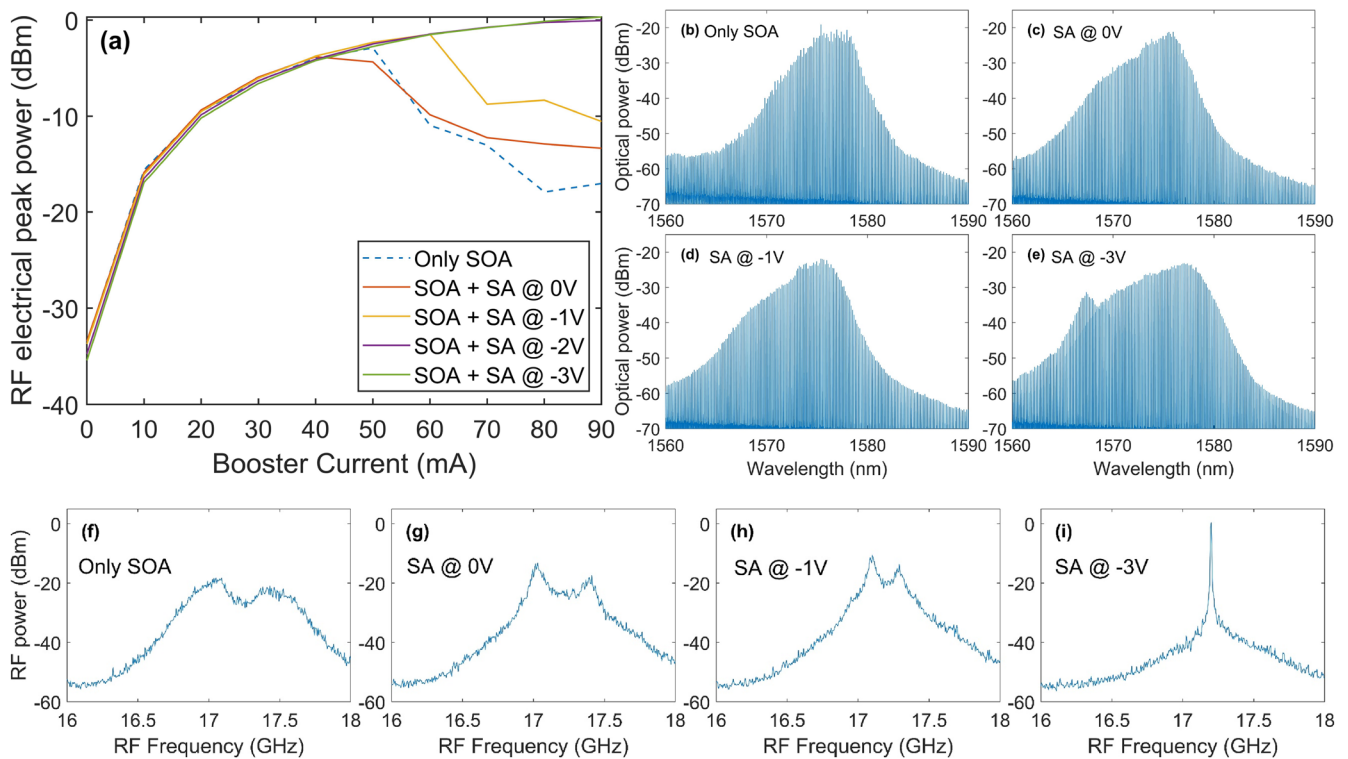


FIG. 3. (a) RF peak power around 17 GHz as a function of booster current for the MLLs combined with the conventional “only SOA” booster (blue dashed line) and with the “custom” booster with a 20 μm -long SA at different bias voltages (solid lines). Output optical/RF spectra at 90 mA booster current for the MLLs followed by the “only SOA” booster (b)/(f) and the “custom” booster with 20 μm -long SA at 0 V (c)/(g), -1 V (d)/(h), and -3 V (e)/(i) reverse bias voltage.

Another crucial parameter for studying the influence of feedback in a ring-cavity MLL with two SOAs is the current balance between the two SOAs. Since the MLL is subjected to a backward-traveling feedback signal from the lensed fiber reflection, one of the SOAs is the first to experience the feedback signal inside the cavity, and in our setup, this is SOA1 [see Fig. 1(a)]. For this reason, the current balance between both SOAs in the cavity, even with a constant total injected current, plays a significant role in the MLL’s sensitivity to destabilization.

To illustrate the importance of the MLL current balance, Fig. 4(a) shows the evolution of the RF peak power for MLLs with “only SOA” and “custom” boosters with 30 μm -long SAs as a function of the booster current while applying 70 mA to SOA1 and 30 mA to SOA2. Figures 4(b) and 4(c) show the same curves, but this time for 50 mA/50 mA and 30 mA/70 mA applied to SOA1 and SOA2, respectively. Hence, Figs. 4(a)–4(c) illustrate three different MLL current balance conditions, with a constant total injected current of 100 mA.

Figure 4(a) presents a balance of 70% (70 mA) injected into SOA1 and 30% (30 mA) into SOA2. This scenario is similar to that of Figs. 2 and 3, and analogously, the “only SOA” booster leads to destabilization of the laser’s pulsing regime above a certain booster current, while the SA-enhanced “custom” booster prevents destabilization over the entire booster current range, achieving higher RF

peak power than the “only SOA” booster. We note that, when applying more current to SOA1 than to SOA2, the laser cavity is very sensitive to feedback. This is a direct consequence of the laser layout, in which the feedback signal first passes through SOA1 and, in view of the high current applied to SOA1, experiences a strong amplification and is more likely to impact the laser’s stability.

In contrast, when the MLL current balance is shifted toward SOA2, for instance, with symmetric injection (50 mA/50 mA), as considered in Fig. 4(b), the curve for the MLL with “only SOA” booster does not exhibit a sharp drop in RF peak power. Nevertheless, the curve still suggests that the laser’s stability is not maintained over the entire booster current range, as the RF peak power levels off around 60 mA, and when verifying the RF spectrum (not shown here), the RF peak is found to broaden but is not yet completely distorted.

When shifting the MLL current balance even more to SOA2 by applying, respectively, 30 mA/70 mA to SOA1/SOA2, as considered in Fig. 4(c), neither the “only SOA” nor the “custom” boosters show signs of MLL destabilization for any booster current value. In this case, the “custom” booster, although more lossy because of the presence of the SA in front of the SOA, yields only slightly lower RF peak powers than the conventional “only SOA” booster.

Figures 3 and 4 demonstrate the effectiveness of the SA-enhanced “custom” booster for different SA lengths and laser

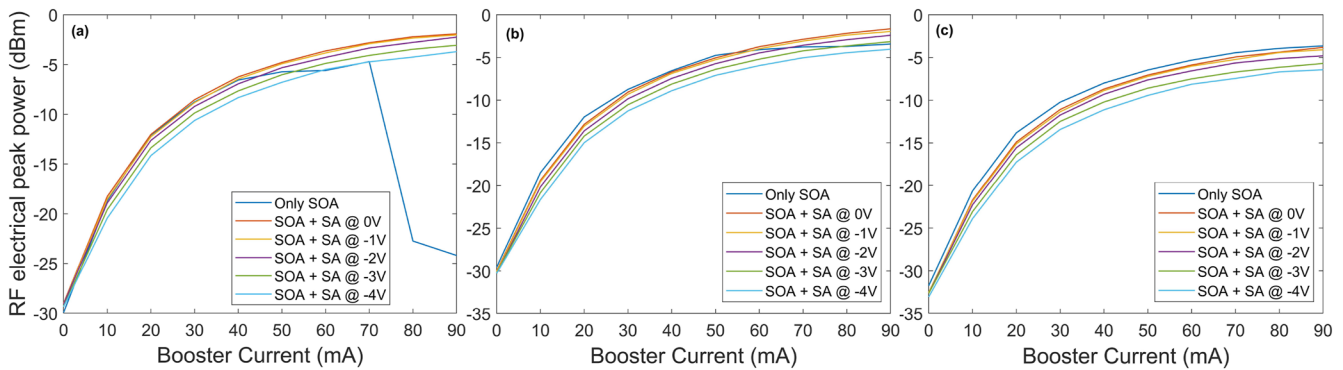


FIG. 4. RF peak power around 17 GHz as a function of booster current for the MLLs combined with the “only SOA” booster and “custom” booster with a 30 μm -long SA, at different MLL current balances between SOA1 and SOA2: (a) 70 mA (SOA1)/30 mA (SOA2), (b) 50 mA/50 mA, and (c) 30 mA/70 mA. The total MLL injected current is kept constant at 100 mA.

driving conditions. Our new booster design successfully suppresses destabilization for the most sensitive configurations while incurring minimal performance penalties for configurations that are less prone to feedback (a more detailed discussion on the performance penalty will follow further on). That said, it should be noted that Figs. 3 and 4 present results for only a limited selection of devices and driving conditions. A comprehensive statistical study covering a larger number of devices on several PICs, operated under a wider range of driving conditions, is required to verify the general validity of our findings.

To this end, we characterize MLLs with “only SOA” and “custom” boosters featuring 20, 30, and 40 μm -long SAs on eight different PICs. We measure their maximum RF peak powers while varying the MLL current balance ratio from 30/70 to 70/30 in 10% increments and while keeping the total injected MLL current fixed at 100 mA. To determine the maximum RF peak powers, we apply for each case the optimal SOA booster current (and, for the “custom” booster, also the optimal SA reverse bias voltage) for which the RF peak power is maximized. The results are summarized in Fig. 5. The data points in Fig. 5 represent the averaged RF peak powers for each configuration, i.e., averaged over eight different PICs, and the error bars denote the standard deviation.

In Fig. 5, we can distinguish three different scenarios: (1) asymmetrical bias in favor of SOA1, e.g., 30% current in SOA2, (2) symmetrical bias, and (3) asymmetrical bias in favor of SOA2, e.g., 70% current in SOA2. In scenario (1), the majority of the current is applied to the SOA that first experiences the feedback signal (SOA1 in our setup, as discussed earlier), while the opposite occurs in scenario (3).

In scenario (1), the SA-enhanced “custom” boosters consistently outperform the conventional “only SOA” booster across all SA lengths, both in averaged RF peak power and in standard deviation. This implies improved stability and reproducibility across the different PICs. The 20 and 30 μm SA-based boosters yield the highest average performance, while the 40 μm SA-based booster achieves the lowest variability, which may benefit stability-critical applications.

Under symmetric bias (2), i.e., scenario (2), the 20 and 30 μm SA-based boosters continue to outperform the “only SOA” booster in terms of both averaged RF peak power and variability. In

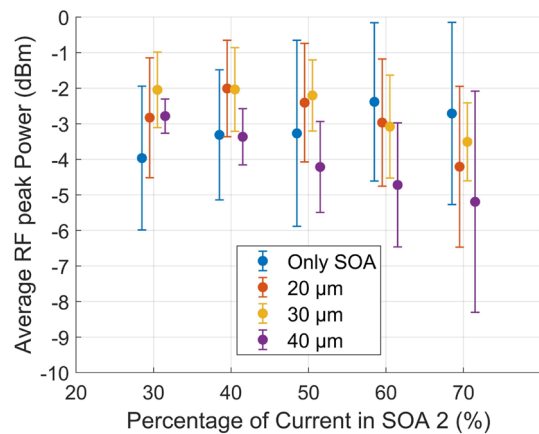


FIG. 5. Statistical analysis of RF peak power around 17 GHz, averaged over 8 PICs, as a function of the percentage of current applied to SOA2, under a constant total MLL current of 100 mA. The results are shown for the “only SOA” booster (blue color) and for the “custom” boosters with 20 (red), 30 (yellow), and 40 μm -long (purple) SAs.

contrast, the 40 μm version falls slightly below the “only SOA” booster in averaged RF peak power; however, it still offers enhanced stability.

In scenario (3), the conventional “only SOA” booster yields the highest averaged RF peak power, but at the cost of significantly increased standard deviation across the different PICs. In contrast, the 30 μm SA-based booster still achieves an averaged RF peak power that is comparable to that of the “only SOA” booster (within 1 dB) while substantially reducing statistical uncertainty. The 40 μm variant, however, offers no additional benefit in this scenario as compared to the “only SOA” booster.

In summary, the statistical analysis presented in Fig. 5 confirms the robustness and reproducibility of stable pulsed lasing with the SA-enhanced “custom” boosters across multiple PICs and current balance ratios, particularly for SA lengths of 20 and 30 μm . A major advantage of the SA-enhanced boosters is that they are

general-purpose building blocks that can be appended not just to symmetrical ring cavity MLLs as considered here but essentially to any integrated pulsed laser in order to solve the feedback problem. It is important to note that the RF peak powers as shown in Fig. 5 serve as a direct indicator of the quality and consistency of the laser's pulsed operation. A comparison based on total optical output power shows that average output powers exceeding 2.6 and 2.4 mW, respectively, can be generated with “only SOA” boosters and “custom” boosters. Hence, the “only SOA” booster can deliver marginally greater optical output powers than the “custom” boosters. However, the highest optical output powers are obtained for high booster currents, where the RF peak power for the “only SOA” booster tends to drop as discussed earlier. For the example above with optical output powers of 2.6 and 2.4 mW for the “only SOA” and “custom” boosters, the RF peak power is more favorable for the “custom” booster by more than 12 dB. This is because the MLL with the “only SOA” booster features unstable pulsing, and its optical output power of 2.6 mW comprises contributions from both CW and pulsed components, which cannot be distinguished by low-bandwidth power meters. Therefore, the optical output power does not provide a reliable measure of the pulsed laser performance for the “only SOA” booster. In contrast, for the “custom” boosters, the RF peak powers remain high even for high booster currents, so that the measured optical output power is due to pulsed laser operation only. The difference in total optical output power (0.2 mW in the example mentioned above) finds its origin in the SAs included in the “custom” boosters, which unavoidably induce some loss. Transmission measurements carried out for stand-alone SAs (20–40 μm in length) with picosecond pulsed input light confirm that this small power penalty is consistent with the SA's induced loss in the saturated regime. Finally, we point out that the loss caused by the SA is only a small fraction of the total amplification enabled by the SA-enhanced custom boosters, which goes up to 7.3 dB for the case with 2.4 mW optical output power.

NUMERICAL SIMULATION RESULTS

To support the experimental results discussed in the previous sections with theoretical insight, we numerically simulate the booster dynamics using an open-source traveling-wave model (TWM) presented in Ref. 21, known as PHIsim.²² The model employs the SOA/SA rate equations presented in Ref. 23, accounting for key nonlinear effects such as two-photon absorption, carrier heating, and free carrier absorption, featuring a quadratic dependence on carrier density.²²

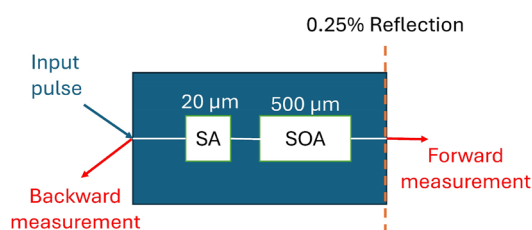


FIG. 6. Schematic illustration of the numerically simulated setup containing an SA-enhanced booster.

TABLE I. Parameters employed in the PHIsim simulation.

Simulation	
Time step (fs)	25.8
Simulated time (ps)	2500
Active region height (nm)	26.5
Active region width (μm)	2
Injected pulse	
Pulse FWHM width (ps)	1
Pulse peak power (mW)	50
Pulse energy (pJ)	0.05
Pulse repetition frequency (GHz)	20
SOA	
Carrier lifetime (ps)	598
Gain coefficient (m^2)	1.694×10^{-19}
Carrier linewidth enhancement factor	4
Carrier temperature linewidth enhancement factor	2
Two photon absorption (cm/GW)	37
ASE coupling factor to SOA (s^{-1})	10×10^{-4}
Free carrier absorption (m^{-1}/m^3)	2.264×10^{-21}
Free carrier absorption quadratic term (m^{-1}/m^6)	-2.502×10^{-46}
SA	
Carrier lifetime (ps)	15
Losses (cm^{-1})	1
Transparency carrier density (m^{-3})	6.577×10^{23}

The simulated setup, represented in Fig. 6, includes an input sech^2 -shaped pulse, a 500 μm -long “only SOA” booster or an SA-enhanced “custom” booster with a 20 μm -long SA and 500 μm -long SOA, a reflection of 0.25%, replicating that produced by the AR-coated lensed fiber employed in the experimental setup, and optical power measurements for the forward and backward propagating signals. The latter corresponds to the feedback signal that, experimentally, would be injected back into the MLL cavity, and the forward propagating signal is the one that would be measured at the output of the chip.

Table I shows the general simulation parameters, as well as the parameter values for the injected pulse, SOA, and SA used in the simulation.²⁴

The simulated performance of the custom SA-enhanced booster relative to the “only SOA” configuration is evaluated in Fig. 7. The blue curve “Only SOA—Custom Booster forward” shows the difference in output pulse power after forward propagation through, respectively, the “Only SOA” booster and “custom” booster. The yellow curve “Only SOA—Custom Booster backward” shows the power difference measured in the backward direction, i.e., after the forward propagating pulse has undergone a 0.25% reflection and subsequently traveled back through the “Only SOA” booster and “custom” booster, respectively. The results indicate that

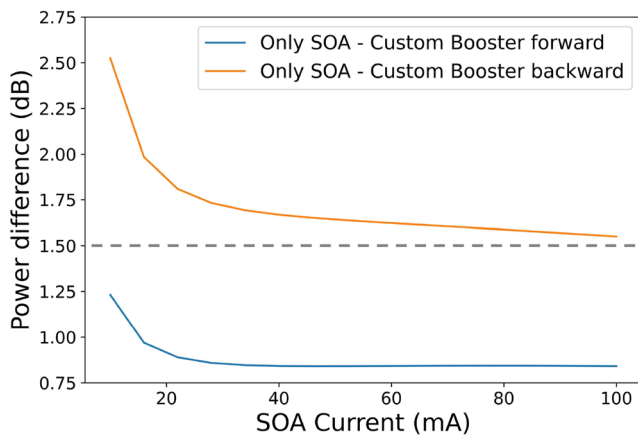


FIG. 7. Simulated difference in optical power for the “Only SOA” booster vs the “custom” booster with 20 μm -long SA, in forward (blue color) and backward (orange) propagation when injecting a 1 ps sech^2 pulse with 50 mW peak power.

the SA of the “custom” booster introduces an insertion loss around 1 dB or less in the forward path, in good agreement with our experimental observations, while simultaneously achieving a reduction of more than 1.5 dB in backward propagating power. This amount of feedback suppression, provided by the short (20 μm) SA of the “custom” booster, turns out to be sufficient to prevent laser destabilization as observed experimentally. Figure 7 also indicates that the feedback suppression exceeds the marginal output power penalty in the forward direction for the SA-enhanced “custom” booster, hence supporting the experimentally observed enhancement in output performance enabled by the “custom” boosters. We note that the feedback suppression represented by the orange curve in Fig. 7 shows a nonlinear dependence on the booster current because of the SA’s intrinsic nonlinear behavior but remains larger than 1.5 dB over the entire booster current range. Our simulation results thus confirm that the SA-enhanced “custom” boosters provide sufficient feedback suppression to enable stable laser pulsing even for the highest booster currents.

SUMMARY AND CONCLUSIONS

In this study, we have introduced a novel SA-enhanced on-chip power booster design that allows amplifying the emission of integrated pulsed lasers, such as MLLs, while suppressing the impact of detrimental optical feedback. Through extensive experimental characterization and numerical simulations, we have demonstrated the effectiveness of the proposed design in comparison with conventional “only SOA” boosters across a wide range of operating conditions and device variants.

Our experimental results show that conventional “only SOA” boosters can induce destabilization of the lasers’ pulsing regime at high booster current levels, leading to a decrease in RF peak output power. In contrast, the proposed SA-enhanced “custom” boosters maintain stable laser operation across the full booster current range, allowing reliable and efficient pulse amplification. These observations are further supported by numerical simulation results, confirming that the proposed “custom” booster design provides

improved feedback isolation toward the laser cavity. In addition, since we can precisely control the reverse bias voltage applied to the SAs in the “custom” boosters, we can effectively mitigate feedback-induced instabilities even in sensitive conditions. Thanks to the nonlinear response of the proposed SA-enhanced booster architecture, robust laser isolation can be provided while minimizing insertion loss.

To validate these findings, we have performed a systematic statistical analysis across multiple PICs, lasers, and operation points. The study reveals that some MLL driving conditions are more sensitive to feedback than others, but generally, the use of an SA-enhanced “custom” booster instead of an “only SOA” booster benefits the robustness and reproducibility of stable pulsed lasing across multiple PICs, particularly for SA lengths of 20 and 30 μm . We note that in cases where more current is injected into SOA1 of the MLL than into SOA2, custom boosters with 20 and 30 μm -long SAs consistently deliver the highest RF peak powers and lowest variability, confirming their effectiveness in both performance and reproducibility.

Notably, although similar optical output powers can be achieved with conventional “only SOA” and “custom” boosters (2.6 and 2.4 mW, respectively, at high booster currents), the “only SOA” booster fails to maintain the pulsing regime in that case, as evidenced by a drop of more than 12 dB in RF peak power compared to the “custom” booster. Hence, its optical output power of 2.6 mW comprises contributions from both CW and pulsed components, whereas the output power of 2.4 mW for the “custom” booster is due to pulsed laser operation only. We also note that the overall signal amplification of the “custom” SA-enhanced booster reaches up to 7.3 dB in that case and that the SA’s power penalty is only on the order of 1 dB or less, as confirmed through numerical simulations.

In summary, the integration of a short SA into on-chip power boosters for integrated MLLs significantly enhances the lasers’ pulsing stability, robustness, and repeatability while allowing for efficient amplification. In view of its simplicity, scalability, and effectiveness, our approach to providing feedback isolation can be very beneficial for feedback-sensitive integrated photonic systems in various application domains, ranging from optical communication and data processing to LiDAR and metrology.

ACKNOWLEDGMENTS

The authors acknowledge financial support from Fonds Wetenschappelijk Onderzoek (Grant Nos. G005420N and G092424N); Vrije Universiteit Brussel-OZR; Ministerio de Ciencia, Innovación y Universidades (Spain) (Grant Nos. PID2021-123459OB-C22MCIN/AEI/FEDER, UE, and CNS2023-143986MICIU/AEI/NextGenerationEU/PRTR).

AUTHOR DECLARATIONS

Conflict of Interest

The authors have no conflicts to disclose.

Author Contributions

D. Plaza-Vas: Conceptualization (equal); Data curation (equal); Formal analysis (equal); Investigation (equal); Methodology

(equal); Software (equal); Validation (equal); Visualization (equal); Writing – original draft (equal). **A. Quirce:** Formal analysis (equal); Methodology (equal); Writing – review & editing (equal). **E. Bente:** Formal analysis (equal); Methodology (equal); Software (equal); Writing – review & editing (equal). **N. Vermeulen:** Conceptualization (lead); Formal analysis (equal); Funding acquisition (lead); Methodology (equal); Project administration (lead); Resources (lead); Supervision (lead); Validation (equal); Writing – review & editing (equal).

DATA AVAILABILITY

The data that support the findings of this study are available from the corresponding author upon reasonable request.

REFERENCES

- ¹H. Zhao, S. Pinna, F. Sang, B. Song, S. T. Suran Brunelli, L. A. Coldren, and J. Klamkin, “High-power indium phosphide photonic integrated circuits,” *IEEE J. Sel. Top. Quantum Electron.* **25**(6), 4500410 (2019).
- ²A. Hermans, K. van Gasse, and B. Kuyken, “On-chip optical comb sources,” *APL Photonics* **7**(10), 100901 (2022).
- ³L. Chang, S. Liu, and J. E. Bowers, “Integrated optical frequency comb technologies,” *Nat. Photonics* **16**, 95–108 (2022).
- ⁴B. Qin, R. Zhang, B. Qiu, B. Zhang, and C. Luo, “Theoretical analysis of passively mode-locked semiconductor ring lasers,” *Opt. Express* **32**(14), 24358–24371 (2024).
- ⁵K. van Gasse, R. Wang, and G. Roelkens, “27 dB gain III–V-on-silicon semiconductor optical amplifier with >17 dBm output power,” *Opt. Express* **27**(1), 293–302 (2019).
- ⁶D. Arsenijević, M. Kleinert, and D. Bimberg, “Phase noise and jitter reduction by optical feedback on passively mode-locked quantum-dot lasers,” *Appl. Phys. Lett.* **103**, 231101 (2013).
- ⁷L. Drzewietzki, S. Breuer, and W. Elsässer, “Timing jitter reduction of passively mode-locked semiconductor lasers by self- and external-injection: Numerical description and experiments,” *Opt. Express* **21**, 16142–16161 (2013).
- ⁸S.-S. Li, V. Pusino, S.-C. Chan, and M. Sorel, “Experimental investigation on feedback insensitivity in semiconductor ring lasers,” *Opt. Lett.* **43**(9), 1974–1977 (2018).
- ⁹G. Verschaffelt, M. Khoder, and G. Van der Sande, “Optical feedback sensitivity of a semiconductor ring laser with tunable directionality,” *Photonics* **6**(4), 112 (2019).
- ¹⁰L. Nielsen, E. A. J. M. Bente, E. den Haan, and M. J. R. Heck, “Theoretical and experimental investigation of unidirectionality in an integrated semiconductor ring mode-locked laser with two saturable absorbers,” *IEEE J. Quantum Electron.* **54**(5), 2000810 (2018).
- ¹¹L. Bi, J. Hu, P. Jiang, D. H. Kim, G. F. Dionne, L. C. Kimerling, and C. A. Ross, “On-chip optical isolation in monolithically integrated non-reciprocal optical resonators,” *Nat. Photonics* **5**, 758–762 (2011).
- ¹²M. Heck, S. Srinivasan, M. Davenport, and J. Bowers, “Integrated microwave photonic isolators: Theory, experimental realization and application in a unidirectional ring mode-locked laser diode,” *Photonics* **2**(3), 957–968 (2015).
- ¹³T. T. M. van Schaijk, D. Lenstra, E. A. J. M. Bente, and K. A. Williams, “Theoretical analysis of a feedback insensitive semiconductor ring laser using weak intracavity isolation,” *IEEE J. Sel. Top. Quantum Electron.* **24**(1), 1800108 (2018).
- ¹⁴D. Lenstra, T. T. M. van Schaijk, and K. A. Williams, “Toward a feedback-insensitive semiconductor laser,” *IEEE J. Sel. Top. Quantum Electron.* **25**(6), 1502113 (2019).
- ¹⁵M. J. R. Heck, E. A. J. M. Bente, Y. Barbarin, D. Lenstra, and M. K. Smit, “Monolithic semiconductor waveguide device concept for picosecond pulse amplification, isolation, and spectral shaping,” *IEEE J. Quantum Electron.* **43**(10), 910–922 (2007).
- ¹⁶M. J. R. Heck, E. A. J. M. Bente, Y. Barbarin, A. Fryda, H.-D. Jung, Y.-S. Oei, R. Nötzel, D. Lenstra, and M. K. Smit, “Characterization of a monolithic concatenated SOA/SA waveguide device for picosecond pulse amplification and shaping,” *IEEE J. Quantum Electron.* **44**(4), 360–369 (2008).
- ¹⁷V. Moskalenko, S. Latkowski, S. Tahvili, T. de Vries, M. Smit, and E. Bente, “Record bandwidth and sub-picosecond pulses from a monolithically integrated mode-locked quantum well ring laser,” *Opt. Express* **22**, 28865–28874 (2014).
- ¹⁸U. Bandelow, M. Radziunas, A. Vladimirov, B. Hüttel, and R. Kaiser, “40 GHz mode-locked semiconductor lasers: Theory, simulations and experiment,” *Opt. Quantum Electron.* **38**, 495–512 (2006).
- ¹⁹X. Tang, J. C. Cartledge, A. Sheen, A. Akrou, and G. Duan, “Low-timing-jitter all-optical clock recovery for 40 Gbit/s RZ-DPSK and NRZ-DPSK signals using a passively mode-locked quantum-dot Fabry-Perot semiconductor laser,” *Opt. Lett.* **34**, 899–901 (2009).
- ²⁰C. Weber, L. Drzewietzki, and S. Breuer, “Amplitude jitter and timing jitter characterization of a monolithic high-power passively modelocked tapered quantum dot laser,” *Proc. SPIE* **9892**, 989225 (2016).
- ²¹E. A. J. M. Bente, Y. Barbarin, M. J. R. Heck, and M. K. Smit, “Modeling of integrated extended cavity InP/InGaAsP semiconductor modelocked ring lasers,” *Opt. Quantum Electron.* **40**, 131–148 (2008).
- ²²E. A. J. M. Bente, “PHIsim—A photonic integrated circuit simulator: PHIsim v3,” (2023); <https://sites.google.com/tue.nl/phism/home?authuser=0>.
- ²³J. M. Tang and K. A. Shore, “Strong picosecond optical pulse propagation in semiconductor optical amplifiers at transparency,” *IEEE J. Quantum Electron.* **34**(7), 1263–1269 (1998).
- ²⁴E. A. J. M. Bente, “PHIsim—A photonic integrated circuit simulator: Parameter input file,” (2023); <https://sites.google.com/tue.nl/phism/home/input-files/parameter-input-file?authuser=0>.